Design, Synthesis, and In Silico Evaluation of Novel Benzimidazole-Based Urea Derivatives Targeting VEGFR-2

Mustafa Ridha Shihan

College of Pharmacy, Ahl Al Bayt University, Kerbala, Iraq

Email: mrsheehan89@gmail.com

Received: 17/04/2026
Accepted: 28/05/2026
Published: 30/06/2026
DOI: https://doi.org/10.65682/kjnhs.v2.i2.166-181

Abstract

Introduction: Angiogenesis (in tumor growth and metastasis) is a fundamental process which is regulated primarily via vascular endothelial growth factor receptor-2 (VEGFR-2). Although VEGFR-2 is a confirmed target in anti-tumor management, available inhibitors currently suffer from many limitations such as drug resistance and dose-related toxicity, so it becomes necessary to develop novel and more safe inhibitors. The aim of this study is to design, synthesize, and evaluate a new series of benzimidazole-urea derivatives (U1–U4) as potential inhibitors of VEGFR-2 with enhanced binding affinity and better drug-likeliness properties.

Methods: Four compounds benzimidazole-urea derivatives were synthesized chemically and analyzed structurally using FT-IR, 1H-NMR, and 13C-NMR spectroscopy. Molecular docking studies were performed against VEGFR-2 (PDB ID: 4ASD) to detect interaction profiles especially binding affinity, with Sorafenib which is used as a reference inhibitor. Physico-chemical properties and pharmacokinetics (ADME) properties were predicted to evaluate drug-likeness and oral bioavailability. Statistical analysis used. Docking scores and binding energies were obtained from molecular docking simulations and analyzed in comparison with the reference drug; no experimental statistical tests were applied.

Results: The four synthesized derivatives exhibited high binding affinities toward VEGFR-2. The best among them were compound U4 which showed the highest docking score (−9.8877 kcal/mol), better than that of Sorafenib (−9.3847 kcal/mol). We identified the key interactions with critical amino acid residues, including Glu885, Asp1046, and Cys919, which indicating stable binding within the ATP-binding pocket. More interesting result were in silico ADME analysis that revealed beneficial physicochemical properties and expected oral bioavailability for all the four synthesized compounds.

Conclusion: The newly synthesized benzimidazole-urea derivatives exhibit potential VEGFR-2 inhibitory activity, favourable binding properties and drug likeliness. These compounds are promising and could be more extensively tested in biological systems as anti-angiogenic and anticancer drugs.

Keywords: Benzimidazole; Sorafenib; Anticancer; VEGFR-2 inhibitors; Urea.

1. Introduction

Although there are many advances in cancer diagnostic and therapeutic protocols, significant needs for unmet treatments remain, specifically for breast, lung, and pancreatic cancers. Ongoing research focuses on developing novel anticancer agents that minimize effects on healthy cells while reducing the risk of secondary malignancie (Ma & Yu, 2007). Given the role of vascular endothelial growth factor (VEGF) in stimulating endothelial cell proliferation, migration, and angiogenesis, VEGF receptors (VEGFR), especially VEGFR-2, have emerged as key targets in anticancer drug development. (Wu et al., 2024) Since VEGFA is a primary mediator of angiogenesis via VEGFR-2, most current antiangiogenic therapies target either VEGFA or VEGFR-2 (Shibuya, 2011). VEGFR2, a tyrosine kinase receptor, activates signaling pathways upon binding VEGFA that promote endothelial cell functions critical for new blood vessel formation. Inhibitors of VEGFR2, also termed kinase insert domain receptor (KDR) inhibitors, function by suppressing angiogenesis and thereby exhibit antitumor activity. These agents are widely utilized in clinical oncology to disrupt tumor vasculature. Consequently, selective inhibition of VEGFR2 represents a promising approach for novel anticancer drug development (Çevik et al., 2025; Elkady et al., 2023; Elzanaty et al., 2024).

Notably, several VEGFR2 inhibitors, including sorafenib, cabozatinib, lenvatinib, and sunitinib, have received approval from the Food and Drug Administration (FDA) (Figure 1) (Iliev et al., 2026; Son et al., 2020).

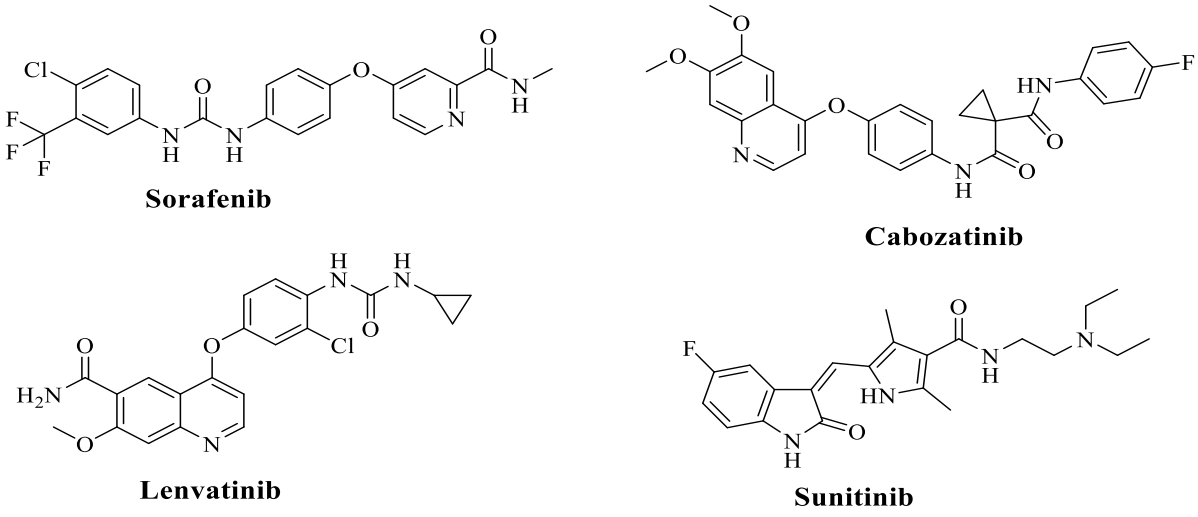

Figure 1. Chemical structure of the clinical approval of several tyrosine kinase inhibitors (TKIs) such as sunitinib, sorafenib and pazopanib**.**

Benzimidazole constitutes a fundamental structural component in various pharmaceuticals, including veliparib, bendamustine, nocodazole, and carbendazim (Figure 2) (Son et al., 2020). Extensive research has examined benzimidazole derivatives for their wide range of biological activities, such as antibacterial, anti-inflammatory, antiallergic, antioxidant, antitubercular, anthelmintic, antimalarial, and anticancer properties (Keshwani et al., 2023; Mayer et al., 2024).

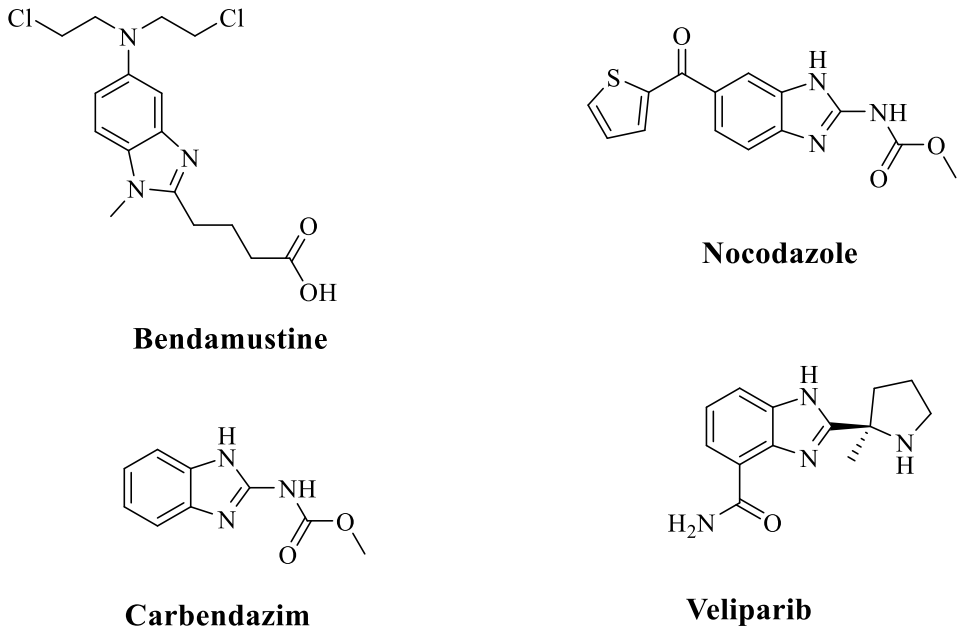

Figure 2. Chemical structure of the veliparib, bendamustine, nocodazole, and carbendazim.

Although VEGFR-2 inhibitors have demonstrated significant therapeutic benefits, their application is limited by challenges such as drug resistance, systemic toxicity, and unsatisfactory pharmacokinetic properties (Manuscript 2014)**.** Therefore, the synthesis of more effective inhibitors of VEGFR-2, more selective, and more safer ones are still in the focus of medicinal chemistry efforts. Due to their strong affinity to the ATP binding site of VEGFR-2, and their important anti-angiogenic property, there has been a considerable number of recent investigations of benzimidazole-based scaffolds (Li et al., 2011). While several benzimidazole derivatives have been explored as VEGFR-2 inhibitors, the novelty of the present study lies in the strategic incorporation of a specific urea linker conjugated with an aromatic amide group. This design aims to provide superior conformational flexibility and extended hydrogen-bonding capabilities within the ATP-binding pocket and the adjacent allosteric hydrophobic regions, potentially overcoming the binding limitations and resistance issues of previously reported benzimidazole scaffolds. By systematically varying the terminal aromatic moieties (phenyl vs. pyridyl) and the N-substitution on the benzimidazole core, these newly designed compounds are hypothesized to achieve enhanced binding affinity and improved pharmacokinetic profiles. Based on these findings, four derivatives (U1–U4) were designed and synthesized as new potentials that have an aromatic amide group which is conjugated to the benzimidazole core to enhance the binding efficiency and selectivity to VEGFR-2. Molecular docking with human VEGFR-2 crystal structure complexed with a type II inhibitor (PDB ID: 4ASD) (Friesner et al., 2006) was used to test the inhibition property of these compounds. The Docking analysis was carried out with Docking software (Auto Dock Vina and Glide algorithms) that showed the favorable binding conformation and interactions at the ATP-binding site, which were mainly composed of the key residues of the ATP-binding site (Cys919, Glu885, Asp1046). The computational results provide deep insights into the mechanism of VEGFR-2 inhibition and highlight the potential of these newly developed compounds as anti-angiogenic agents.

2. Subjects and Methods

General procedure to synthesis benzimidazole derivatives (U1-U4) (Chfat et al., 2025) The urea derivatives U1–U4 were synthesized via the condensation reaction of 5-methoxy-1-methyl-1H-

benzo[d]imidazol-2-amine or 5-methoxy-1H-benzo[d]imidazol-2-amine with the appropriate isocyanate derivatives (N-(4-isocyanatophenyl)acetamide or N-(6-isocyanatopyridin-3-yl)acetamide) in dry dichloromethane under an inert atmosphere. Typically, the benzimidazole amine (1.0 mmol) was dissolved in 15 mL of dry dichloromethane, and the corresponding isocyanate (1.1 mmol) was added dropwise at room temperature, while stirring. This reaction mixture was stirred for 4-5 hours and the progress of the reaction was followed by TLC until the starting material was completely consumed. The solvent evaporated under reduced pressure, and the crude product was washed with cold water, dried and purified by recrystallization from ethyl acetate or by column chromatography (hexane/ethyl acetate gradient) to yield solid products of the desired urea derivatives U1-U4. The synthesized compounds have been characterized by IR, ^{1}H NMR, and ^{13}C NMR which confirmed that the urea linkage has been successfully formed and the presence of characteristic methoxy, amide, and aromatic functional groups.

N-(4-(3-(5-methoxy-1-methyl-1*H*-benzo[d]imidazol-2-yl)ureido)phenyl) acetamide (U1): Pale yellow solid; yield 65%; Mp: 179–181 °C; FTIR (cm^{-1}, υ) 3324, 3338 (N–H, urea and acetamide), 1657 (C=O amide), 1679 (–CH=CH–aromatic ring); ^{1}H NMR (300 MHz, DMSO-d_6, δ ppm): 10.57 (s, 1H, NH of urea linked to imidazole ring), 10.01 (s, 1H, NH of urea attached linked to pyridine ring), 9.68 (s, 1H,NH of acetamide group), 7.65 – 7.21 (m, 7H, aromatic protons), 3.86 (s, 3H, -O-CH_3), 3.64 (s, 3H, -CH_3 linked to imidazole ring), 2.07 (s, 3H, -CH_3 of acetamide); ^{13}C NMR (75 MHz, DMSO-d_6) δ 170.23(1C, of carbonyl acetamide),156.54(1C, of carbonyl acetamide), 153.87, 146.67, 141.72, 136.94, 133.05, 131.03, 123.79, 121.21, 116.07, 112.54, 109.47 (13C, aromatic carbons), 56.14(1C, -O-CH_3), 33.87(1C, -CH_3 linked to imidazole ring), 23.42(1C, -CH_3 of acetamide).

N-(4-(3-(5-methoxy-1*H*-benzo[d]imidazol-2-yl)ureido)phenyl)acetamide (U2): White solid; yield 70%; Mp: 166–168 °C; FTIR (cm^{-1}, υ) 3345, 3312,3217 (N–H, urea, acetamide and imidazole ring), 1675 (C=O amide), 1694 (–CH=CH–aromatic ring); ^{1}H NMR (300 MHz, DMSO-d_6, δ ppm): 11.89(s, 1H, NH of imidazole ring), 11.57 (s, 1H, NH of urea linked to imidazole ring), 9.98 (s, 1H,NH of acetamide group), 9.73 (s, 1H, NH of urea attached linked to pyridine ring), 7.74 – 7.08 (m, 7H, aromatic protons), 3.83(s, 3H, -O-CH_3), 2.06 (s, 3H, -CH_3 of acetamide); ^{13}C NMR (75 MHz, DMSO-d_6) δ 168.34(1C, of carbonyl acetamide), 157.08 (1C, of carbonyl acetamide), 153.92, 148.87, 139.47, 137.14, 133.65, 130.05, 124.88, 121.22, 118.29, 113.88, 110.21(13C, aromatic carbons), 55.39(1C, -O-CH_3), 24.12(1C, -CH_3 of acetamide).

N-(6-(3-(5-methoxy-1-methyl-1*H*-benzo[d]imidazol-2-yl)ureido)pyridin-3-yl)acetamide (U3): White solid; yield 71%; Mp: 131–133 °C; FTIR (cm^{-1}, υ) 3344, 3362 (N–H, urea, and acetamide), 1664 (C=O amide), 1681(–CH=CH–aromatic ring); ^{1}H NMR (300 MHz, DMSO-d_6, δ ppm): 10.87 (s, 1H, NH of urea linked to imidazole ring), 10.52 (s, 1H, NH of urea attached linked to pyridine ring), 9.84 (s, 1H,NH of acetamide group), 8.04 – 7.27 (m, 6H, aromatic protons), 3.89 (s, 3H, -O-CH_3), 3.68 (s, 3H, -CH_3 linked to imidazole ring), 2.12 (s, 3H, -CH_3 of acetamide); ^{13}C NMR (75 MHz, DMSO-d_6) δ 169.12 (1C, of carbonyl acetamide),155.97(1C, of carbonyl acetamide), 153.53, 150.79, 146.58, 143.17, 141.95, 131.03, 129.46, 127.96, 118.07, 114.32, 112.00, 110.26 (12C, aromatic carbons), 55.92(1C, -O-CH_3), 34.54(1C, -CH_3 linked to imidazole ring), 24.21(1C, -CH_3 of acetamide).

N-(6-(3-(5-methoxy-1*H*-benzo[d]imidazol-2-yl)ureido)pyridin-3-yl)acetamide (U4): Pale white solid; yield 67%; Mp: 147–149 °C; FTIR (cm^{-1}, υ) 3311, 3329, 3238 (N–H, urea, acetamide and imidazole ring), 1681 (C=O amide), 1685(–CH=CH–aromatic ring); ^{1}H NMR (300 MHz,

DMSO-d_6, δ ppm): 11.97 (s, 1H, NH of imidazole ring), 11.47 (s, 1H, NH of urea linked to imidazole ring), 11.14 (s, 1H, NH of urea attached linked to pyridine ring), 9.92 (s, 1H,NH of acetamide group), 8.11 – 7.14 (m, 6H, aromatic protons), 3.87 (s, 3H, -O-CH_3), 2.11 (s, 3H, -CH_3 of acetamide); ^{13}C NMR (75 MHz, DMSO-d_6) δ 168.59(1C, of carbonyl acetamide),156.47 (1C, of carbonyl acetamide), 152.18, 149.79, 144.60, 141.16, 138.34, 133.54, 129.46, 127.82, 120.29, 116.29, 112.88, 108.01(12C, aromatic carbons), 55.22(1C, -O-CH_3), 24.23(1C, -CH_3 of acetamide).

2.1. Molecular docking procedure

The 4ASD coordinate file was downloaded from the PDB database from the protein preparation (VEGFR-2). Then we did inspection to the structure and removal of all non-essential heteroatoms and ligands except that for any crystallographic waters or cofactors (in this study HOH2142 was retained because it gave conserved interactions). Missing side chains and loops were added, assigning correct protonation states for ionizable residues at neutral pH 7.4, then optimizing hydrogen bonding network. Minimizing the protein briefly to relieve bad contacts while preserving the backbone conformation.

2.2. Ligand preparation (U1–U4, Sorafenib)

The ligands U1–U4 and Sorafenib (the reference drug) were prepared using the Molecular Operating Environment (MOE, version 2015). In Chem Draw the 2D chemical structures were drawn and imported into MOE in. mol format, then they were converted in MOE into 3D geometries utilizing the Builder module. Every structure was confirmed for correct valence hybridization, and connectivity before applying the Protonate 3D tool to give protonation states consistent with physiological pH (7.4). Partial atomic charges were calculated automatically using the MMFF94x force field. Geometry optimization was performed through energy minimization using the same force field with a gradient convergence criterion of 0.001 kcal/mo l Å to obtain stable low-energy conformations. Optional conformational search was performed to find the lowest energy conformer for each compound. The optimized structures of the ligands were then saved as .mdb format for docking in MOE and then exported as. mol2 or PDB format for compatibility with the molecular docking protocol using VEGFR-2 receptor (PDB ID: 4ASD).

2.3. Docking Validation Procedure

To ensure the reliability and scientific rigor of the molecular docking protocol, a redocking validation process was performed. The native co-crystallized ligand (Sorafenib) was extracted from the active site of the VEGFR-2 crystal structure (PDB ID: 4ASD) and subsequently redocked into the same binding pocket using the identical parameters employed for the tested compounds. The validity of the docking procedure was confirmed by calculating the Root Mean Square Deviation (RMSD) between the predicted best-docked pose and the native experimental co-crystallized conformation. An RMSD value of less than 2.0 Å was considered the acceptable validation criterion, verifying that the applied docking algorithm accurately reproduces the experimental binding mode.

3. Results

The synthesized urea derivatives, U1–U4 (Figures 4-7) were successfully obtained in moderate to good yield (65–71%) as pure white to pale-yellow crystalline solids with well-defined melting point which is indicative of the purity and stability of the synthesized urea derivatives. The FTIR spectra of all compounds exhibited characteristic absorption bands in the range of 3310–3362 cm^{-1}, attributed to N–H stretching vibrations of urea, acetamide, and imidazole groups, indicating the

successful formation of the urea linkage. The strong bands around 1650–1690 cm^{-1} correspond to the C=O stretching of the amide and urea carbonyl groups, while additional absorptions at 1680–1695 cm^{-1} were assigned to aromatic C=C stretching, confirming the presence of conjugated aromatic systems. The ^{1}H NMR spectra provided clear evidence for the formation of the target compounds through the appearance of multiple downfield singlets between 10.0–12.0 ppm, corresponding to the NH protons of the imidazole, urea, and acetamide functionalities. The aromatic protons appeared in region of 7.1–8.1 ppm as multiplets, with the presence of substituted aromatic and heteroaromatic rings. As well, singlets at 3.8–3.9 ppm indicates the methoxy (–OCH_3) group, while in U1 and U3 peaks at 3.6–3.7 ppm were corresponded to the methyl group attached to the imidazole nitrogen, confirming N-methyl substitution. The methyl protons of acetamide resonated consistently around 2.1 ppm, supporting the presence of this moiety. The ^{13}C NMR spectrum more verified these conclusions, showing characteristic carbonyl carbons(C=O) of the acetamide and urea groups between 168–170 ppm and 155–157 ppm, respectively. The carbon signals of aromatic ring appeared between 110–150 ppm, revealing the presence of benzimidazole, phenyl, and pyridyl rings. Peaks at 55 ppm refer to the methoxy carbon, while those at 24 ppm refer to acetamide methyl carbon. Compounds U1 and U3 also showed an additional signal at 34 ppm that for methyl group attached to the imidazole nitrogen. Comparatively, small changes in the spectra of U1-U4 indicate comparatively small changes in electronic environments resulting from the changes in substitution patterns and heteroaromatic bonds, (phenyl vs. pyridyl; N-methylated vs. non-methylated benzimidazole). The melting points of U1 (179-181 °C) and U2 (166-168 °C) are higher than those of U3 (131-133 °C) and U4 (147-149 °C) suggesting that the intermolecular hydrogen bonding and crystallinity of the phenyl-based derivatives are stronger. The general trends from the data obtained from FTIR, ^{1}H NMR, and ^{13}C NMR confirm the successful synthesis and structural integrity of the four ureas synthesized. All the observed peaks show the presence of all the expected functional groups and the observed chemical shifts indicate the actual coupling between the benzimidazole and the aromatic isocyanate derivatives via ureas, supporting the proposed molecular structures for U1–U4.

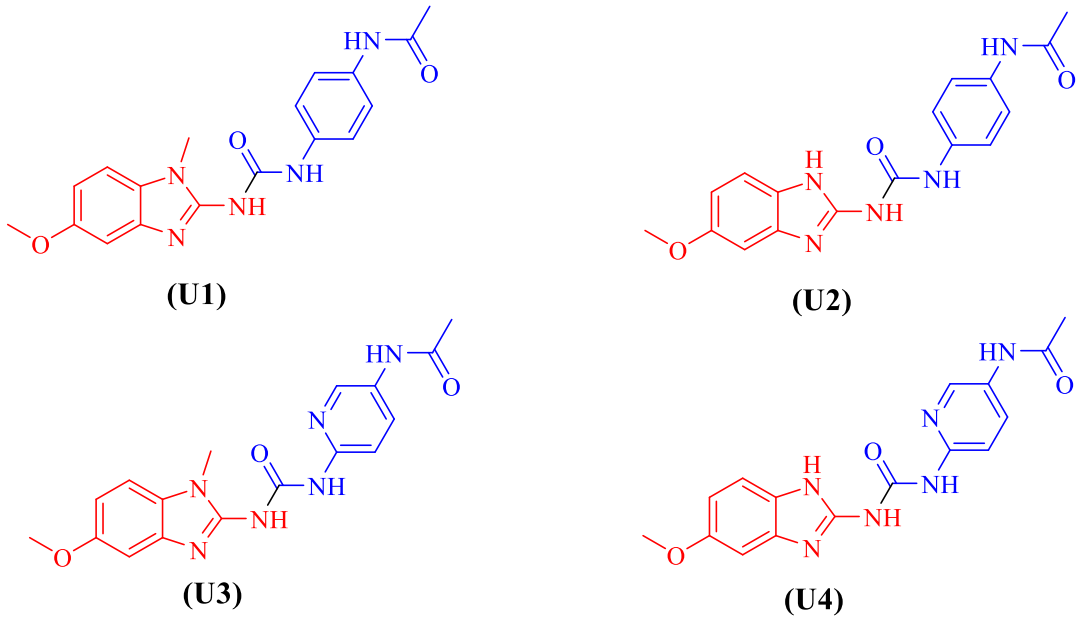

Figure 3. The chemical structure of the prepared compounds (U1-U4).

3.1. Docking studies

The molecular docking results of the synthesized compounds U1–U4 and the reference drug Sorafenib with the VEGFR-2 (PDB ID: 4ASD) receptor is summarized in Table 1. The docking scores and interaction profiles showed that all compounds had good docking scores for VEGFR-2 similar or lower to Sorafenib in the active site. From the designed ligands, U4 has the most favorable docking score (−9.8877 kcal/mol) when compared with Sorafenib (−9.3847 kcal/mol) which suggests that U4 is having a strong binding affinity and it is interacting in a stable manner with receptor ATP binding site. Additionally, compound U1 (−8.0611 kcal/mol) and compound U2 (−7.4703 kcal/mol) showed important interactions and were able to make multiple hydrogen bonds with some of the essential amino acid sites such as: Glu885, Asp1046, and HOH2142, which are known to play an important role in VEGFR-2 inhibition. Interestingly, U3 made both hydrogen bond donor (H-B-D) and acceptor (H-B-A) contacts with Glu885, Asp1046, and HOH2142, although with a somewhat weaker docking score, indicating that there is moderate binding affinity. The RMSD values of all the ligands were within the highly acceptable range (0.7037–1.5940 Å), which is well below the standard validation threshold of 2.0 Å. This statistical validation metric confirms the accuracy of the docking protocol, ensuring that the predicted interactions are highly reliable and indicating stable docking poses. The interactions found were hydrogen bonds and π–H contacts, which play important roles in the stabilization of ligand–receptor complexes. The contacts with Cys919 in Sorafenib and Glu885 in all the compounds tested highlight the conserved binding mode inside the kinase domain. The hydrogen bond between the urea or amide group of the prepared ligands with Asp1046 provide further stability in binding to the ATP site by docking deeply into the site. Overall, the results of the docking indicated that the designed benzimidazole–urea derivatives, especially the U4 compound, have good inhibitory activity towards VEGFR-2 and can be used as lead compounds for further modification in order to develop novel anti-angiogenic drugs.

Table 1. Molecular docking scores and binding interactions of ligands (U1–U4) and Sorafenib against VEGFR-2 (PDB: 4ASD).

Ligand	RMSD (Å)	Dock Score (E, kcal·mol⁻¹)	Interaction type (per interaction)	ΔE (kcal·mol⁻¹) per interaction	Distance (Å)	Residue / Partner
U1	1.2906	−8.3364	H-B-D	−2.0	2.92	HOH 2142
			H-B-D	−5.0	2.92	GLU 885
			H-B-A	−2.0	2.87	ASP 1046
U2	1.5586	−8.0611	H-B-D	−2.0	2.91	HOH 2142
			H-B-D	−5.2	2.93	GLU 885

Ligand	RMSD (Å)	Dock Score (E, kcal·mol⁻¹)	Interaction type (per interaction)	ΔE (kcal·mol⁻¹) per interaction	Distance (Å)	Residue / Partner
			H-B-A	−0.7	3.19	SYS 1045
			H-B-A	−2.1	3.01	ASP 1046
			π–H	−0.8	4.42	SYS 1045
U3	0.7037	−7.4703	H-B-D	−2.5	3.28	GLU 885
			H-B-D	−0.3	3.99	HOH 2142
			H-B-A	−1.2	2.93	ASP 1046
			π–H	−1.0	3.74	LEU 840
			π–H	−0.7	4.16	LEU 840
U4	1.5940	−9.8877	H-B-D	−5.2	2.93	GLU 885
			H-B-D	−2.3	2.89	HOH 2142
			H-B-A	−2.1	3.02	ASP 1046
			π–H	−0.8	4.43	ASP 1046
Sorafenib	1.4284	-9.3847	H-B-D	−0.8	2.96	CYS 919
			H-B-D	−2.0	2.97	HOH 2142
			H-B-D	−3.9	2.97	GLU 885
			H-B-A	−2.6	3.29	CYS 919
			H-B-A	−2.0	2.89	ASP 1046

* Note: Legend: H-B-D = hydrogen bond donor; H-B-A = hydrogen bond acceptor; π–H = π–hydrogen interaction; HOH 2142 = crystallographic water molecule 2142.

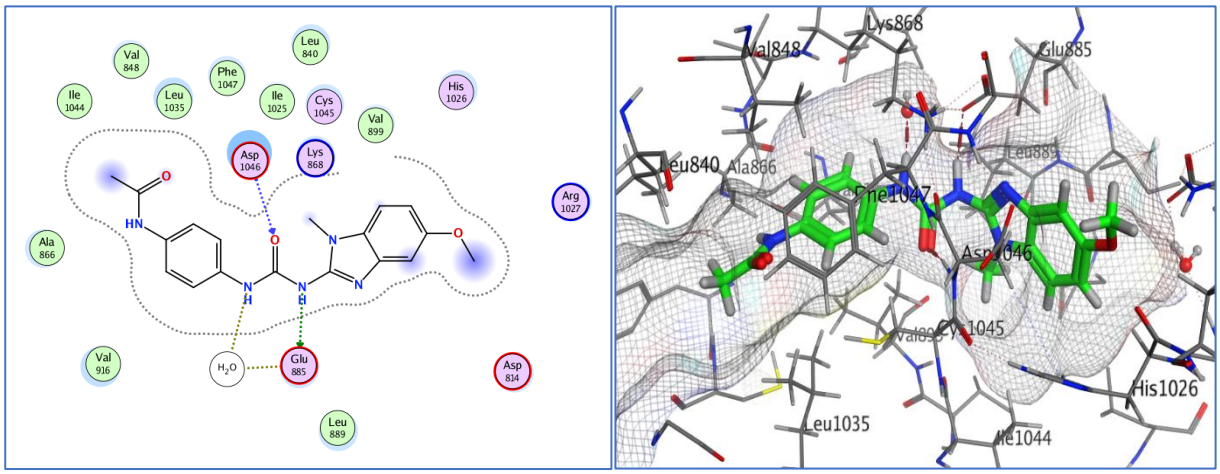

Figure 4. Three-dimensional (3D) and two-dimensional (2D) representations of the docking interactions between compound U1 and the active site residues of (PDB ID: 4ASD).

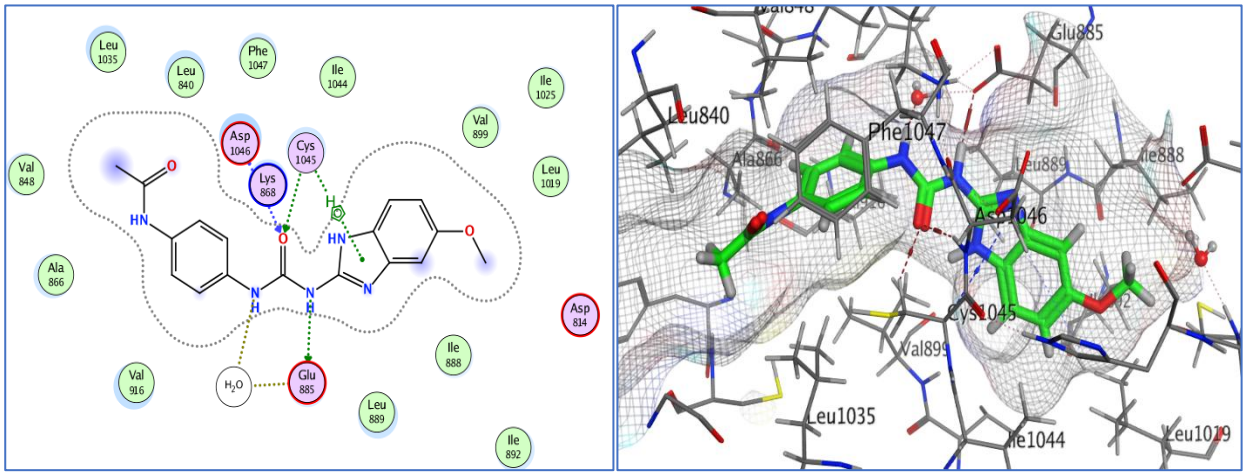

Figure 5. Three-dimensional (3D) and two-dimensional (2D) representations of the docking interactions between compound U2 and the active site residues of (PDB ID: 4ASD).

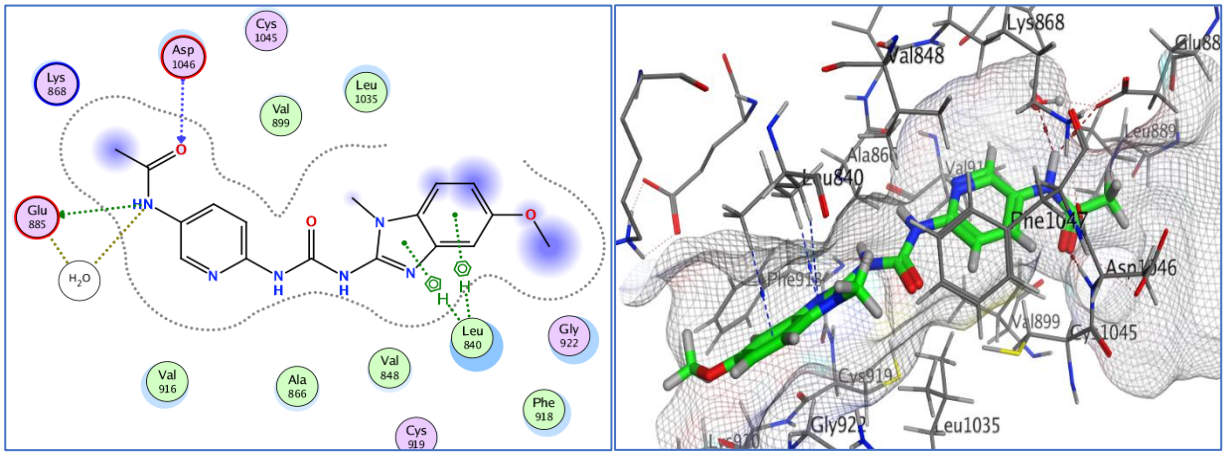

Figure 6. Three-dimensional (3D) and two-dimensional (2D) representations of the docking interactions between compound U3 and the active site residues of (PDB ID: 4ASD).

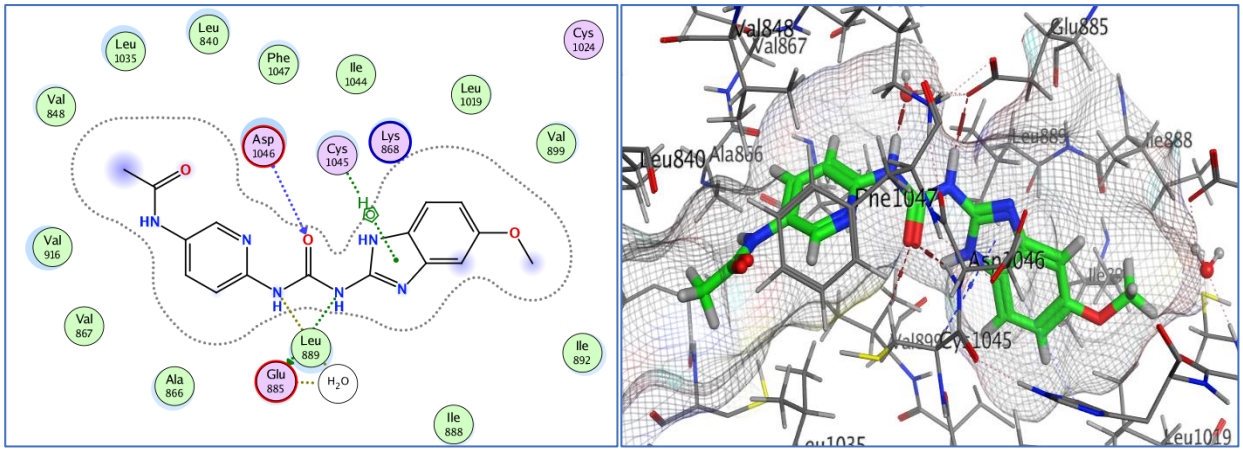

Figure 7. Three-dimensional (3D) and two-dimensional (2D) representations of the docking interactions between compound U4 and the active site residues of (PDB ID: 4ASD).

3.2. Physicochemical and ADME profiles

The radar plots presented in Figure 8 provide a comparative overview of the predicted oral bioavailability profiles of Sorafenib and the synthesized compounds U1–U4 across multiple pharmacokinetic parameters. The analysis shows that all four derivatives have good bioavailability properties with the most of them having values in the good range for oral drug-like properties. Synthesized compounds U2 and U4 have the most well-balanced profiles with a good predicted absorption, moderate lipophilicity, and suitable molecular flexibility, which are important parameters for effective gastrointestinal absorption. Both U1 and U3 are slightly different from the classic drugs in terms of such parameters as topological polar surface area (TPSA) or hydrogen bond donors/acceptors, but still within acceptable ranges, indicating that they might have adequate oral absorption. In comparison, Sorafenib has a well characterized oral bioavailability profile but the radar plots suggest that some of the synthesized derivatives, especially U4, may show a better or similar pharmacokinetic profile. Overall, these findings suggest that the designed benzimidazole–urea derivatives retain potent VEGFR-2 inhibitory potential as evidenced by docking, as well as promising oral bioavailability properties and are thus promising candidates for further in vivo pharmacokinetic and efficacy evaluation.

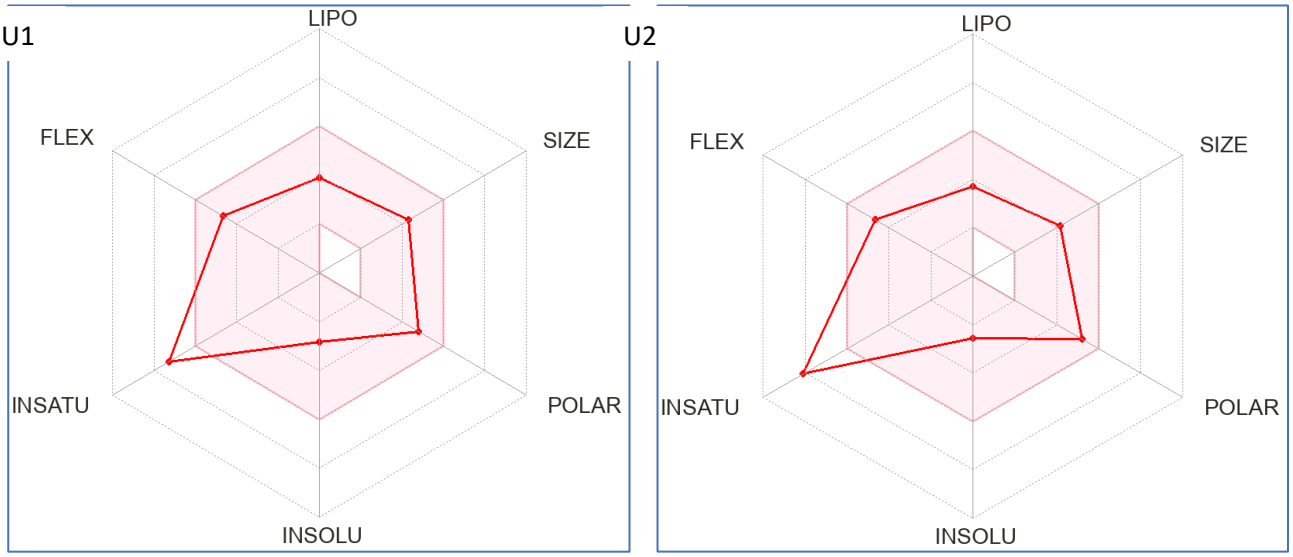

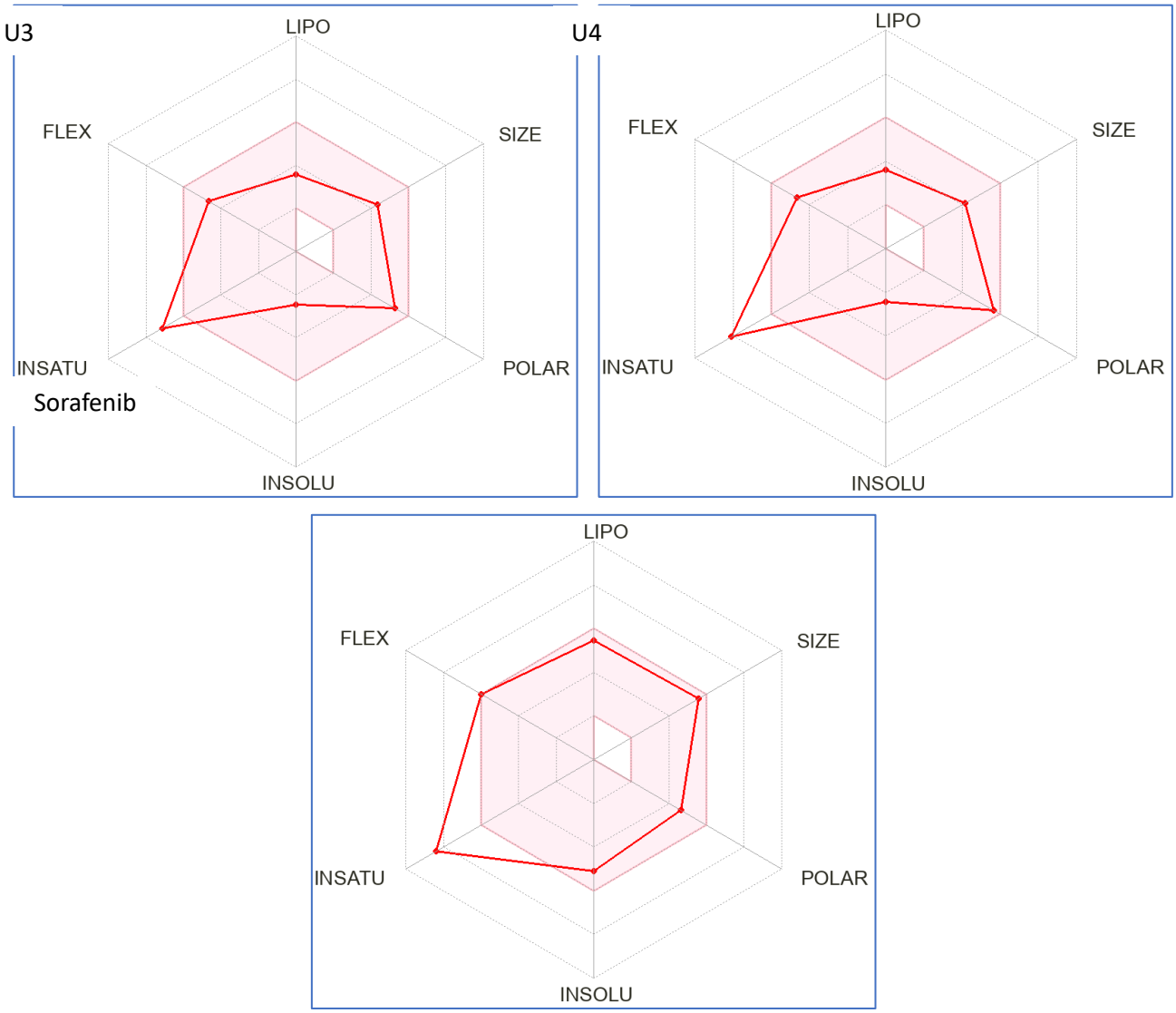

Figure 8. Radar plots depicting the predicted oral bioavailability profiles of Sorafenib and the synthesized compounds U1, U2, U3, and U4, highlighting key pharmacokinetic parameters.

As can be seen in Table 2, the physicochemical and ADME properties of the synthesized compounds U1–U4 in comparison with Sorafenib gives valuable information about the drug-likeness and potential pharmacokinetic behavior. The molecular weights of the derivatives are 339–354 g/mol, lower than Sorafenib (464.82 g/mol) that might be beneficial for absorption and distribution. The number of heavy atoms and rotatable bonds for U1–U4 are slightly less than those of Sorafenib, suggesting possible better molecular flexibility and membrane permeability. Hydrogen bond donors and acceptors are within acceptable ranges with U2 and U4 having slightly more H-bond donors (4) that could increase specific interactions with biological targets, but may make it a little more permeable. The predicted high gastrointestinal (GI) absorption for U1-U4 (97-121 Å²), which are in the range of the topological polar surface area (TPSA) values of good oral absorption (generally <140 Å²), is in accordance with this fact, while there is slightly lower GI absorption for Sorafenib. The lipophilicity of all the derivatives is calculated by multiple methods (iLOGP, XLOGP3, WLOGP, MLOGP) and found to be moderate for all of them, showing that derivatives U1 and U2 are more lipophilic than derivatives U3 and U4. All the compounds are non-conformant with Lipinski's and Veber's rules for drug-likeness.

In terms of metabolism, all compounds are predicted not to pass the blood–brain barrier (BBB), which lowers the risk of central nervous system (CNS) side effects. U1, U3 and U4 are likely P-glycoprotein (P-gp) substrates and may affect efflux and bioavailability while with respect to Sorafenib, this is not anticipated to affect efflux and bioavailability. CYP450 inhibition profiles show selective inhibition patterns (U1 and U4 inhibit CYP2D6, but other CYP isoforms are little affected compared to Sorafenib which inhibits multiple CYP isoforms), which means that metabolic drug–drug interactions are likely to be less of a concern than with Sorafenib. Finally, all of the compounds have the same bioavailability score of 0.55, which is considered to have moderate potential for oral bioavailability. The results indicate that U1-U4 has good physicochemical properties and also advantageous over Sorafenib in terms of molecular weight, GI absorption and lower CYP related metabolic drawbacks and hence are promising for future pharmacokinetic and in vivo testing.

Table 2. Physicochemical properties and ADME (Absorption, Distribution, Metabolism, and Excretion) profiles of the synthesized compounds U1-U4 and the reference drug Sorafenib.

Molecules	**U1**	**U2**	**U3**	**U4**	**Sorafenib**
MW	353.38	339.35	354.36	340.34	464.82
Heavy atoms	26	25	26	25	32
Rotatable bonds	7	7	7	7	9
H-bond acceptors	4	4	5	5	7
H-bond donors	3	4	3	4	3
TPSA	97.28	108.14	110.17	121.03	92.35
iLOGP	1.44	1.58	1.96	1.13	3.42
XLOGP3	1.29	0.99	0.75	0.79	4.07
WLOGP	2.61	2.6	2.01	2	6.32
MLOGP	1.38	1.14	0.36	0.12	2.91
GI absorption	High	High	High	High	Low
BBB permeant	No	No	No	No	No
Pgp substrate	Yes	Yes	Yes	Yes	No
CYP1A2 inhibitor	No	Yes	No	No	Yes
CYP2C19 inhibitor	No	No	No	No	Yes
CYP2C9 inhibitor	No	No	No	No	Yes
CYP2D6 inhibitor	Yes	Yes	No	No	Yes
CYP3A4 inhibitor	No	No	No	No	Yes
Lipinski violations	0	0	0	0	0
Veber violations	0	0	0	0	0
Bioavailability Score	0.55	0.55	0.55	0.55	0.55

4. Discussion

The U1–U4 series was prepared by the rational design and validation of scaffolds, which proved to be a very efficient approach in our research. In medicinal chemistry, benzimidazole is known as a "privileged scaffold", owing to its structural similarity to purine, which enables binding at the ATP binding site of many kinases (Wagh & Kankate, 2025). Adding a urea linker follows a well-known approach in designing VEGFR-2 inhibitors; prior studies indicate the urea group acts as a crucial "bridge" that helps inhibitors reach from the ATP-binding pocket into the hydrophobic allosteric back pocket, which is key for strong binding (Eldehna et al., 2016). Our spectroscopic data are consistent with the integration of this linker in U1-U4 with the correct orientation for deep receptor interaction.

4.1. Molecular Docking and Binding Mechanism

In particular it is interesting to consider the molecular docking of compound U4 (−9.8877 kcal/mol), which is related to the mechanism of action of kinases. The interactions seen between U4 and Glu885 and Asp1046 suggest that these derivatives are Type II kinase inhibitors. According to the reports of structural biology, the Type II inhibitors stabilize the inactive conformation of the kinases by forming hydrogen bond with the conserved DFG motif (Asp-Phe-Gly) (Vijayan et al., 2015). The contact with Asp1046 is of special importance as it represents an indicator of stable, deep-pocket contact, which impedes the activation loop from being returned to its active conformation (Modi & Kulkarni, 2019). This is in contrast to Type I inhibitors that only bind the active kinase conformation. Interestingly, U4 seems to mimic the binding mode of Sorafenib, which binds the DFG-out state, by binding to the same residues (Cys919 and Asp1046), but with a higher docking score, indicating it may be more potent (Hasegawa et al., 2007).

4.2. Focused on Clinical Limitations: Resistance and Safety.

The development of new VEGFR-2 inhibitors is driven by the need to overcome the limitations of current drugs, like Sorafenib. While effective, Sorafenib's therapeutic efficacy is often undermined after 6 months of treatment because of drug resistance, which is often associated with mutations in the ATP-binding cleft (Tang et al., 2020). Moreover, the broad spectrum of inhibition of Sorafenib may cause severe off-target side effects such as hypertension and hand-foot syndrome (J. Li et al. 2024). Based on our in silico ADME analyses, compounds U1–U4 could have a more favourable safety profile. The latter can be distinguished from Sorafenib, which inhibits multiple CYP450 isoforms, by the fact that these derivatives are selective inhibitors of CYP2D6 and therefore have a reduced risk of complex metabolic drug-drug interactions, which is important for patients with cancer who are taking combination treatments (Properties, 2008) .

4.3. Overall Summary and Study Limitations

In summary, this study successfully designed and synthesized a novel series of benzimidazole-urea derivatives (U1-U4). The computational findings emphasize that integrating the urea moiety significantly enhances binding interactions with crucial amino acid residues (particularly Glu885 and Asp1046), effectively mimicking the deep-pocket binding characteristic of Type II kinase inhibitors. Furthermore, the ADME predictions present a promising pharmacokinetic profile with anticipated oral bioavailability and a reduced potential for multi-CYP inhibition compared to existing therapies like Sorafenib. However, it is imperative to acknowledge the limitations of the current study. The findings discussed herein are fundamentally based on *in silico* molecular docking simulations and

computational ADME predictions. While these computational tools are robust for initial screening and structural optimization, the biological activity, therapeutic efficacy, and safety profile of the synthesized compounds have not yet been experimentally validated. Future investigations must prioritize extensive *in vitro* enzymatic assays to determine the precise IC50 values against VEGFR-2, followed by *in vivo* biological evaluations. Acquiring experimental structural data will also be critical to definitively substantiate the proposed binding mechanisms and translate these computational findings into clinical applications. (Eldehna et al., 2016; Properties, 2008) .

5. Conclusions

Overall, the study was able to successfully design and synthesize a novel series of benzimidazole-urea derivatives (U1–U4) as potential anti-angiogenic agents targeting VEGFR-2. All compounds were spectrally characterized and purified. The molecular docking simulation results showed that these compounds have good binding affinity and interaction with the ATP binding pocket of VEGFR-2 compared to the reference drug Sorafenib with the highest docking score of U4. The residues, Glu885, Asp1046 and Cys919 were found to play crucial role for stabilizing the ligand-receptor complexes. Moreover, no violation of Lipinski rules or Veber rules was observed in the all-synthesized derivatives and in silico ADME calculation shows promising drug-like properties and acceptable oral bioavailability for all derivatives. All these observations highlight the potential of the benzimidazole-urea scaffold, notably U4, as a promising lead to develop next generation VEGFR-2 inhibitors. These compounds are predicted to be very potent inhibitors and have good pharmacokinetic properties and are worthy of further study in both in vitro and in vivo settings to assess their therapeutic efficacy and safety for anticancer use.

6. Acknowledgement

I owe my gratitude to the Department of Pharmaceutical Chemistry, Alkafeel University/College of Pharmacy for giving me facilities and technical assistance for carrying out this work. The staff of the laboratory centres for their help with the spectroscopic measurements (1H NMR, 13C NMR and FTIR) and the computational chemistry unit for providing the assistance to carry out the molecular docking study using MOE software are gratefully acknowledged. To Dr. Ali Jabbar Radhi for his efforts and encouragement to do this research.

7. References

Çevik, U. A., Celik, I., Görgülü, Ş., Şahin İnan, Z. D., Bostancı, H. E., Karayel, A., Özkay, Y., & Kaplancıklı, Z. A. (2025). Novel Benzimidazole–Oxadiazole Derivatives as Anticancer Agents with VEGFR2 Inhibitory Activity: Design, Synthesis, In Vitro Anticancer Evaluation, and In Silico Studies. *ACS Omega*, *10*(7), 6801–6813. https://doi.org/10.1021/acsomega.4c08885

Chfat, H. G., Radhi, A. W., Radhi, A. J., & Alrubaie, I. (2025). Design, synthesis, In Silico and in vitro studies urea derivatives as VEGFR-2 inhibitors. *Journal of Molecular Structure*, *1343*, 142863. https://doi.org/10.1016/j.molstruc.2025.142863

Eldehna, W. M., Abou-Seri, S. M., El Kerdawy, A. M., Ayyad, R. R., Hamdy, A. M., Ghabbour, H. A., Ali, M. M., & A. Abou El Ella, D. (2016). Increasing the binding affinity of VEGFR-2 inhibitors by extending their hydrophobic interaction with the active site: Design, synthesis and biological evaluation of 1-substituted-4-(4-methoxybenzyl)phthalazine derivatives. *European Journal of Medicinal Chemistry*, *113*, 50–62. https://doi.org/10.1016/j.ejmech.2016.02.029

Elkady, H., Abuelkhir, A. A., Rashed, M., Taghour, M. S., Dahab, M. A., Mahdy, H. A., Elwan, A., Al-ghulikah, H. A., Elkaeed, E. B., Ibrahim, I. M., Husein, D. Z., Metwaly, A., & Eissa, I. H. (2023). New thiazolidine-2,4-diones as effective anti-proliferative and anti-VEGFR-2 agents: Design, synthesis, in vitro, docking, MD simulations, DFT, ADMET, and toxicity studies. *Computational Biology and Chemistry*, *107*, 107958. https://doi.org/10.1016/j.compbiolchem.2023.107958

Elzanaty, K. A., Omran, G. A., Elmahallawy, E. K., Albrakati, A., Saleh, A. A., Dahran, N., Alhegaili, A. S., Salahuddin, A., Abd-El-Azim, H., Noreldin, A., & Okda, T. M. (2024). Design and Optimization of Sesamol Nanosuspensions to Potentiate the Anti-Tumor Activity of Epirubicin against Ehrlich Solid Carcinoma-Bearing Mice. *Pharmaceutics*, *16*(7), 937. https://doi.org/10.3390/pharmaceutics16070937

Friesner, R. A., Murphy, R. B., Repasky, M. P., Frye, L. L., Greenwood, J. R., Halgren, T. A., Sanschagrin, P. C., & Mainz, D. T. (2006). Extra Precision Glide: Docking and Scoring Incorporating a Model of Hydrophobic Enclosure for Protein−Ligand Complexes. *Journal of Medicinal Chemistry*, *49*(21), 6177–6196. https://doi.org/10.1021/jm051256o

Hasegawa, M., Nishigaki, N., Washio, Y., Kano, K., Harris, P. A., Sato, H., Mori, I., West, R. I., Shibahara, M., Toyoda, H., Wang, L., Nolte, R. T., Veal, J. M., & Cheung, M. (2007). Discovery of Novel Benzimidazoles as Potent Inhibitors of TIE-2 and VEGFR-2 Tyrosine Kinase Receptors. *Journal of Medicinal Chemistry*, *50*(18), 4453–4470. https://doi.org/10.1021/jm0611051

Iliev, I., Nesheva, A., Mavrova, A., Yancheva, D., Kostadinova, A., Semkova, S., Momchilova, A., Tsoneva, I., Staneva, G., & Nikolova, B. (2026). Anticancer Potential of Thieno[2,3-d]pyrimidine Derivatives in Oral Carcinoma Models. *Molecules*, *31*(3), 397. https://doi.org/10.3390/molecules31030397

Keshwani, L., Daniel, K., Daniel, V., & Jain, S. K. (2023). Synthesis and characterization of novel benzimidazole derivative as potent anthelmintic agent. *Current Science*, *3*(2), 300–307.

Li, Y., Tan, C., Gao, C., Zhang, C., Luan, X., Chen, X., Liu, H., Chen, Y., & Jiang, Y. (2011). Discovery of benzimidazole derivatives as novel multi-target EGFR, VEGFR-2 and PDGFR kinase inhibitors. *Bioorganic & Medicinal Chemistry*, *19*(15), 4529–4535. https://doi.org/10.1016/j.bmc.2011.06.022

Ma, X., & Yu, H. (2007). Global burden of cancer. *The Yale Journal of Biology and Medicine*, *79*(3–4), 85.

Mayer, J. C. P., Pereira, P. C., Sagrilo, P. L., Iglesias, B. A., Back, D. F., da Rocha, V. N., Köhler, M. H., Rodrigues, O. E. D., & Dornelles, L. (2024). Synthesis, spectroscopic, electrochemistry and antioxidant properties of benzofuroxan and 2H-benzimidazole 1,3-dioxide derivatives: Effects of conjugation with electron-acceptor 1,2,3-triazolyl-1,2,4-oxadiazole. *Journal of Molecular Structure*, *1311*, 138420. https://doi.org/10.1016/j.molstruc.2024.138420

Modi, S. J., & Kulkarni, V. M. (2019). Vascular Endothelial Growth Factor Receptor (VEGFR-2)/KDR Inhibitors: Medicinal Chemistry Perspective. *Medicine in Drug Discovery*, *2*, 100009. https://doi.org/10.1016/j.medidd.2019.100009

Properties, E. (2008). *Drug-like Properties: Concepts Structure Design and Methods: from ADME to Toxicit Optimization Methods: from ADME to Toxicity Optimization*.

Shibuya, M. (2011). Vascular Endothelial Growth Factor (VEGF) and Its Receptor (VEGFR) Signaling in Angiogenesis: A Crucial Target for Anti- and Pro-Angiogenic Therapies. *Genes & Cancer*, *2*(12), 1097–1105. https://doi.org/10.1177/1947601911423031

Son, D.-S., Lee, E.-S., & Adunyah, S. E. (2020). The antitumor potentials of benzimidazole anthelmintics as repurposing drugs. *Immune Network*, *20*(4), e29.

Tang, W., Chen, Z., Zhang, W., Cheng, Y., Zhang, B., Wu, F., Wang, Q., Wang, S., Rong, D., Reiter, F. P., De Toni, E. N., & Wang, X. (2020). The mechanisms of sorafenib resistance in hepatocellular carcinoma: theoretical basis and therapeutic aspects. *Signal Transduction and Targeted Therapy*, *5*(1), 87. https://doi.org/10.1038/s41392-020-0187-x

Vijayan, R. S. K., He, P., Modi, V., Duong-Ly, K. C., Ma, H., Peterson, J. R., Dunbrack, R. L. Jr., & Levy, R. M. (2015). Conformational Analysis of the DFG-Out Kinase Motif and Biochemical Profiling of Structurally Validated Type II Inhibitors. *Journal of Medicinal Chemistry*, *58*(1), 466–479. https://doi.org/10.1021/jm501603h

Wagh, D. D., & Kankate, R. S. (2025). Benzimidazole Derivatives in Anticancer Therapy: A Comprehensive Review. *Biosciences Biotechnology Research Asia*, *22*(3), 849.

Wu, Y., Sun, J., Lin, Q., Wang, D., & Hai, J. (2024). Sustained release of vascular endothelial growth factor A and basic fibroblast growth factor from nanofiber membranes reduces oxygen/glucose deprivation-induced injury to neurovascular units. *Neural Regeneration Research*, *19*(4), 887–894. https://doi.org/10.4103/1673-5374.382252